JBC Papers in Press. Published on June 21, 2012 as Manuscript M112.382291
The latest version is at http://www.jbc.org/cgi/doi/10.1074/jbc.M112.382291

Conformational Selection and Substrate Binding Regulate the Monomer/Dimer Equilibrium of the C-terminal domain of *Escherichia coli* Enzyme I

Vincenzo Venditti and G. Marius Clore[1]

From the Laboratory of Chemical Physics, National Institute of Diabetes and Digestive and Kidney Diseases, National Institutes of Health, Bethesda, Maryland 20892-0520, USA.

Running title: Conformational dynamics of *E. coli* EIC

[1]Address correspondence to: G. Marius Clore, Laboratory of Chemical Physics, Building 5, National Institute of Diabetes and Digestive and Kidney Diseases, National Institutes of Health, Bethesda, Maryland 20892-0520, USA. Tel.: 301-496-0788; Fax: 301-496-0825. E-mail: mariusc@mail.nih.gov.

Key words: conformational selection / Enzyme I / phosphoenolpyruvate:sugar phosphotransferase system / conformational dynamics / NMR / relaxation dispersion / residual dipolar couplings

Background: Conformational changes in the EIC domain of Enzyme I upon ligand binding are thought to regulate the phosphotransfer system by modulating the monomer/dimer equilibrium.
Results: Binding of phosphoenolpyruvate shifts a pre-existing conformational equilibrium in EIC.
Conclusion: Conformational selection provides a direct structural link between ligand binding and dimer affinity.
Significance: Isolated EIC is an optimal system for investigating dynamic processes regulating EI.

The bacterial phosphotransferase system (PTS) is a signal transduction pathway that couples phosphoryl transfer to active sugar transport across the cell membrane. The PTS is initiated by the binding of phosphoenolpyruvate (PEP) to the C-terminal domain (EIC) of Enzyme I (EI), a highly conserved protein that is common to all sugar branches of the PTS. EIC exists in a dynamic monomer/dimer equilibrium that is modulated by ligand binding, and is thought to regulate the overall PTS. Isolation of EIC has proven challenging, and conformational dynamics within the EIC domain during the catalytic cycle are still largely unknown. Here we present a robust protocol for expression and purification of recombinant EIC from *E. coli*, and show that isolated EIC is capable of hydrolyzing PEP. NMR analysis and residual dipolar coupling measurements indicate that the isolated EIC domain in solution adopts a stable tertiary fold and quaternary structure that is consistent with previously reported crystallographic data. NMR relaxation dispersion measurements indicate that residues around the PEP binding site and in the β3α3 turn (residues 333-366), which is located at the dimer interface, undergo a rapid transition on the sub-millisecond time scale (with an exchange rate constant of ~1500 s^{-1}) between major open (~97%) and minor closed (~3%) conformations. Upon PEP binding, the β3α3 turn is effectively locked in the closed state by the formation of salt bridges between the phosphate group of PEP and the side chains of Lys340 and Arg358, thereby stabilizing the dimer.

Enzyme I (EI)[1] is the first protein in the bacterial phosphoenolpyruvate:sugar phospho-transferase system (PTS), a signal transduction pathway that couples phosphoryl transfer through a series of bimolecular protein-protein complexes to sugar transport across the membrane (1,2). The PTS is also involved in the regulation of diverse cellular processes including transcription, chemotaxis, and glycolysis (2). There are four sugar-specific branches of the PTS, but all require EI to initiate the phosphoryl transfer cascade. EI is autophosphorylated by phosphoenolpyruvate (PEP) and subsequently donates the phosphoryl group to the histidine phosphocarrier protein HPr (3,4). EI and HPr are common to all branches of the PTS. Thereafter, the phosphoryl group is transferred from HPr to the sugar specific enzymes II, and ultimately onto the incoming sugar. It has been recently shown that, under conditions of nitrogen limitation, EI is inhibited by α -ketoglutarate (5), the carbon substrate for ammonia assimilation, thereby providing a regulatory link between central carbon and

Downloaded from www.jbc.org at National Institutes of Health Library, on June 21, 2012

Copyright 2012 by The American Society for Biochemistry and Molecular Biology, Inc.

nitrogen metabolism in bacteria. EI is ubiquitous in bacteria and does not have any eukaryotic counterparts. Thus, given the central role of EI in the control and regulation of bacterial metabolism, it is no surprise that EI has been described as an ideal pharmaceutical target for the identification of novel and highly specific antimicrobials (6).

The functional form of EI is a ~128 kDa dimer of identical subunits (7) comprising two structurally and functionally distinct domains (8,9). The N-terminal phosphoryl-transfer domain (EIN, residues 1-249) contains the site of phosphorylation (His189) and the binding site for HPr (8,10,11). The C-terminal domain (EIC, residues 261-575) is responsible for dimerization and contains the binding site for PEP (12-14). The EIN and EIC domains are connected to one another (15-18) by a long helical linker.

The isolated EIN domain can transfer a phosphoryl group to HPr, but only intact dimeric EI can be autophosphorylated by PEP (8,9,13,19-21). It has therefore been suggested that the monomer/dimer equilibrium for the EIC domain plays a central role in the regulation of the overall PTS (22). Indeed, the interaction of EI with the physiological ligands for the EIC domain, Mg^{2+} and PEP, decreases the equilibrium dissociation constant for dimerization (K_D) by approximately thirty-fold (from 4.8 to 0.15 μM (14,22). Given the intracellular EI concentration of ~10 μM subunits (23), binding of Mg^{2+} and PEP to EI results in a significant shift in the monomer/dimer equilibrium and a concomitant substantial increase in the cellular population of dimeric EI (from ~60 to 90%).

There is now a wealth of structural studies on EI. The isolated EIN domain from *E. coli* has been solved in its free form by crystallography (10) and NMR (11), and in its phosphorylated state (24) and bound to HPr (25) by NMR. In all three cases, the structure of the EIN domain and the relative orientation of the α and α/β subdomains remain unchanged. There are three crystal structures of intact EI, two of free EI from *Staph. Carnosus* (26) and *Staph. Aureus* (16), and one of a trapped phosphorylated intermediate of *E. coli* EI bound to the inhibitor oxalate (15). In addition, there are two solution structures of *E. coli* EI, free and bound to HPr, determined by the combined use of NMR and X-ray scattering (17,18). The EI structures reveal large rigid body conformational transitions involving domain reorientation of EIN relative to EIC, as well as reorientation of the two subdomains of EIN relative to each other. These large scale conformational changes permit transfer of the phosphoryl group from PEP bound to the EIC domain to His189 located on EIN in the conformation found in the trapped phosphorylated intermediate (15), and subsequent transfer of the phosphoryl group on His189 to HPr in the conformation found in the structures of free EI and the EI-HPr complex where the structure of the EIN domain is identical to that of the isolated EIN domain (17). In addition, crystal structures of the isolated EIC domain from *Thermoanaerobacter Tengcongensis* in the free form (27) and in complexes with PEP and pyruvate (28) have been obtained. Although the structure of the EIC domain is the same in intact EI and the isolated EIC domain, spectroscopic and kinetic investigations have suggested that in solution the EIC domain may be present as an ensemble of different conformations that are not apparent in the crystal structures (14).

The recombinant *E. coli* EIC domain has been reported to be proteolytically unstable and difficult to isolate (14,29). Here we present a robust protocol for expression and purification of recombinant *E. coli* EIC. We show that the purified protein adopts a single, stable fold in solution, and is able to hydrolyze PEP into pyruvate and inorganic phosphate. Using relaxation dispersion NMR spectroscopy (30,31) we demonstrate the existence of a rapid local conformational transition on the sub-millisecond time scale between two states, a major open state and a minor closed state, involving residues in the vicinity of the active site. Chemical shift analysis indicates that the conformation of the minor species is similar to that of the PEP-bound state, indicating that PEP binding likely proceeds via conformational selection. Further, in combination with the available crystal structures, the data provide a rationale for understanding dimer stabilization by PEP. The data presented here suggest that EIC represents a good model system for studying the combined effects of substrate binding and conformational dynamics on enzymatic regulation.

Experimental Procedures

Protein expression and purification – Intact EI (residues 1-575) and the EIN domain (residues 1-249) were expressed and purified as previously described (17,24). The EIC domain (residues 261-575) was cloned into a pET11a vector (Novagen) without tags. The plasmid was introduced into *E.*

Downloaded from www.jbc.org at National Institutes of Health Library, on June 21, 2012

coli strain BL21star(DE3) (Invitrogen) and the transformed bacteria were plated onto an LB-agar plate containing ampicillin (100 µg/ml) for selection. Cell were grown at 37°C in either Luria Bertani (LB) or minimal medium (with $^{15}NH_4Cl$ and $^{13}C_6$-glucose as the sole nitrogen and carbon sources, respectively) in H_2O or D_2O, respectively. At A_{600} ~ 0.4 (for LB cultures) or A_{600} ~ 0.8 (for cultures in minimal medium) the temperature was reducedto 20°C and expression was induced with 1 mM isopropyl-D-thiogalactopyranoside (IPTG). Cells were harvested by centrifugation after 16 h of induction and the pellet was resuspended in 20 ml of 20 mM Tris, pH 8.0, 2 mM dithiothreitol (DTT), 1 mM ethylenediaminetetraacetic acid (EDTA), and 1 mM phenylmethylsulfonyl fluoride (PMSF). The suspension was lysed using a microfluidizer and centrifuged at 70,000g for 40 min. The supernatant was filtered and loaded onto a DEAE anion exchange column (20 ml; GE Healthcare), and the protein was eluted with a 400 ml gradient of 1 M NaCl. The fractions containing the protein were confirmed by SDS-polyacrylamide gel electrophoresis and purified by gel filtration on a Superdex-75 column (GE Healthcare) equilibrated with 20 mM Tris, pH 7.4, 200 mM NaCl, 2 mM DTT, and 1 mM EDTA. Relevant fractions were loaded on a monoQ anion exchange column (GE Healthcare), and the protein was eluted with a 400 ml gradient from 150 mM to 400 mM NaCl.

NMR spectroscopy - All the NMR samples were prepared in 20 mM Tris buffer, pH 7.4, 100 mM NaCl, 4 mM $MgCl_2$, 1 mM EDTA, 2 mM DTT, and 90% H_2O/10% D_2O (v/v). The protein concentration (in subunits) was 300-400 µM unless stated otherwise.

NMR spectra were recorded at 37°C on Bruker 900 and 600 MHz spectrometers equipped with either a *z*-shielded gradient triple resonance cryoprobe or, for ^{31}P NMR, an *x*,*y*,*z*-shielded gradient quadruple resonance probe. Spectra were processed using NMRPipe (32) and analyzed using the program SPARKY (http://www.cgl.ucsf.edu/ home/sparky).

Sequential $^1H/^{15}N/^{13}C$ backbone assignment of the EIC domain was carried out using transverse relaxation optimized (TROSY) versions (33,34) of conventional 3D triple resonance correlation experiments (HNCO, HNCA, HNCACB, HN(CO)CA, and HN(CO)CACB) (35). The $^1H/^{15}N/^{13}C$ backbone chemical shifts have been deposited in the BioMagResBank (36) (accession number: 18392). Assignment of the ^1H_N-^{15}N correlations for the EIC-PEP complex was performed by titration experiments, following the change in ^1H-^{15}N cross-peak positions as a function of added PEP in ^1H-^{15}N TROSY spectra. Weighted combined $^1H/^{15}N$ chemical shift perturbations ($\Delta_{H/N}$) resulting from the addition of 10 mM PEP were calculated using the equation (37): $\Delta_{H/N} = [(\Delta\delta_H W_H)^2 + (\Delta\delta_N W_N)^2]^{1/2}$, where W_H and W_N are weighting factors for the ^1H_N and ^{15}N amide shifts, respectively ($W_H = 1$, $W_N = 0.154$), and $\Delta\delta_H$ and $\Delta\delta_N$ are the ^1H_N and ^{15}N chemical shift differences in ppm, respectively, between free and bound states.

Backbone amide $^1D_{NH}$ residual dipolar couplings (RDCs) were measured by taking the difference in $^1J_{NH}$ scalar couplings in aligned and isotropic media (38). The alignment media employed was phage *pf1* (14 mg/ml for EIC and 18 mg/ml for the EIC-PEP complex; ASLA Biotech) (39,40), and $^1J_{NH}$ couplings were measured using the ARTSY pulse scheme (41). Singular value decomposition (SVD) analysis of RDCs was carried out using Xplor-NIH (42).

Relaxation dispersion experiments were conducted using a pulse sequence that measures the exchange contribution for the TROSY component of the ^{15}N magnetization (43). Off-resonance and pulse imperfections effects were minimized using a four-pulse phase scheme (44). Carr-Purcell-Meinboom-Gill (CPMG) experiments were performed at 600 and 900 MHz with a fixed relaxation delay but a changing number of refocusing pulses to achieve different effective CPMG fields (45). The transverse relaxation periods were set to 40 and 20 ms at 600 MHz and 900 MHz, respectively. The effective CPMG fields employed were 100, 200, 300, 400, 500, 600, 700, 800, 900, 1000 Hz at 600 MHz, and 200, 400, 600, 800, and 1000 Hz at 900 MHz. The resulting relaxation dispersion curves were fit to a two-state exchange process using the equation (46,47):

$$R_2(\nu_{cpmg}) = R_2^0 + \frac{p_B(1-p_B)\Delta\omega_N^2}{k_{ex}}\left(1 - \frac{4\nu_{cpmg}\tanh(k_{ex}/4\nu_{cpmg})}{k_{ex}}\right) \quad (1)$$

where R_2^0 is the transverse ^{15}N R_2 in absence of exchange; p_B the relative population of the minor populated state; $\Delta\omega_N$ the ^{15}N chemical shift difference between the two states; k_{ex} the exchange rate constant (given by the sum of the

Downloaded from www.jbc.org at National Institutes of Health Library, on June 21, 2012

forward and backward rate constants k_{AB} and k_{BA} for the transitions from the major species A to the minor species B and back; and υ_{cpmg} the CPMG field defined as $1/2\tau_{cp}$, where τ_{cp} is the spacing between the centers of successive 180° refocusing pulses in the CPMG pulse sequence (45).

Activity assay – Enzymatic activity of EI and EIC for the hydrolysis of PEP to inorganic phosphate and pyruvate were assayed spectrophotometrically at 37°C using the EnzChek Phosphate Assay Kit (Invitrogen) and a nanodrop 2000 spectrophotometer. The reaction mixtures were prepared as follow: 25 µl of 20X reaction buffer from the kit (1.0 M Tris-HCl, 20 mM $MgCl_2$, pH 7.5, 2 mM sodium azide), 7.9 µl of 5 M NaCl, x µl PEP, y µl enzyme, 362.1 - x - y µl doubly distilled H_2O. The mixtures were pre-incubated at 37°C for 10 min prior to the addition of either EI or EIC at a final concentration of ~ 5 µM. For the following 4 hours 39.5 µl aliquots of the reaction mixture were taken at regular intervals and incubated for 10 min with 10 µl of 1 mM 2-amino-6-mercapto-7-methylpurine riboside (MESG) and 0.5 µl of 10 U/ml purine nucleoside phosphorylase (PNP). In the presence of PNP, MESG quantitatively reacts with inorganic phosphate to generate ribose 1-phosphate and 2-amino-6-mercapto-7-methylpurine. Enzymatic conversion of MESG results in a spectrophotometric shift in maximum absorbance from 330 nm for MESG to 360 nm for 2-amino-6-mercapto-7-methylpurine.

Enzymatic assays for EI and EIC were run in duplicate and the obtained A_{360}'s were converted to µmol units using a calibration curve generated from the standard solution of inorganic phosphate provided by the kit. Initial velocities were determined from the linear portion of the progress curves, and were fit by the Michaelis-Menten equation.

Results and Discussion

Expression and isolation of recombinant E. coli EIC — Expression of recombinant *E. coli* EIC (residues 261-575), without addition of any affinity or solubility tag, is described in the *Experimental Procedures*. Purification of EIC from the cell lysate was carried out using a three-step chromatography protocol: weak anion exchange, size exclusion, and a final purification step with a strong anion exchanger (for details see *Experimental Procedures*). Although the first anion exchange step allowed separation of EIC from most of the nucleic acid and protein contaminants, size exclusion chromatography was the key for successful purification of a stable EIC sample. EIC elutes from a Superdex 75 size exclusion column as two partially resolved peaks that have retention volumes of ~125 ml and ~150 ml, referred to as species 1 and 2, respectively, in Fig. 1A.

The final anion exchange step on species 1 reveals the presence of at least four similarly populated EIC isoforms, eluting between 250-350 mM NaCl (Fig. 1B), and the ^{1}H-^{15}N TROSY correlation spectrum obtained on a combined sample of these isoforms shows very poor cross-peak dispersion (Fig. 1D). These data indicate that EIC from species 1 is largely unfolded.

In contrast the anion exchange profile for species 2 is dominated by a major peak eluting at ~300 mM NaCl (Fig. 1C), and the ^{1}H-^{15}N TROSY spectrum acquired for this species is highly dispersed (Fig. 1E), indicative of a stably folded protein. EIC purified from species 2 (note that a slower salt gradient centered at 300 mM NaCl was needed to completely remove contaminations arising from species 1 – see *Experimental Procedures*) is > 90% pure (as determined by SDS-PAGE) and is stable for more than three weeks at 37°C in the presence of 4 mM Mg^{2+}. Moreover, mutation of Met469, which is localized at the dimer interface, to the unnatural amino acid *p*-acetyl-*L*-phenylalanine (a construct not used in the present study) results in large chemical shift perturbations in the $^{1}H_N/^{15}N$ cross-peaks of opposing residues in the other subunit (48), and the overlay of the EI and EIC ^{1}H-^{15}N correlation spectra shows excellent agreement with only small differences in cross-peak positions (Fig 1E). These data clearly indicate that, in the presence of 4 mM $MgCl_2$ and 100 mM NaCl, the isolated EIC domain is a dimer with the same fold as that in the full length EI.

Solution tertiary structure of free E. coli EIC — Crystallographic data show that *E. coli* EIC is a ~ 70 kDa dimer exhibiting an $(\alpha/\beta)_8$ barrel fold with the active site Cys502 located in the β7 α7 turn (15). Comparison of the X-ray structures of *T. Tengcongensis* EIC free and bound to PEP indicates that substrate binding causes rearrangements of a few side chains (Arg296, Phe354, Gln458, Arg465, Met466, and Glu504) in the active site but leaves the overall tertiary fold and quaternary structure unperturbed (28). By way of contrast, sedimentation velocity and thermal denaturation experiments have shown that the addition of PEP stabilizes the protein fold and

Downloaded from www.jbc.org at National Institutes of Health Library, on June 21, 2012

decreases the equilibrium dissociation constant for dimerization (14). PEP binding also results in marked changes in the near UV CD and fluorescence spectra, suggesting that EIC undergoes conformational rearrangements upon PEP binding (14). These spectroscopic techniques, however, only provide averaged information on aromatic side chains, so that one cannot ascertain whether the observed spectral changes reflect global effects or local conformational transitions.

Here we investigate the effect of PEP on the solution structure *E. coli* EIC by NMR. ^{1}H, ^{15}N, and ^{13}C backbone resonances of free EIC were assigned for 278 out of 316 amino acids. The backbone ψ/ϕ torsion angles derived from the backbone chemical shifts using the program TALOS+ (49) are in excellent agreement with the X-ray structure of the trapped phosphorylated intermediate of *E. coli* EI (15) (Fig. 2A). Thus one can conclude that the tertiary structure of the isolated EIC domain in solution is essentially the same as that in the crystal structure of full length EI. $^{1}H_N/^{15}N$ cross-peaks for several residues located in the PEP binding site (Val428-Thr432, Gly452-Tyr559, Cys502-Glu504) are not visible in the ^{1}H-^{15}N TROSY spectrum of EIC, indicating that this region of the protein is undergoing a conformational transition on the sub-millisecond to millisecond time scale (i.e. intermediate exchange on the chemical shift time scale resulting in line-broadening beyond the level of detection).

Relaxation dispersion on free EIC — To characterize the dynamics in the region of the PEP binding site, we carried out Carl-Purcell-Meiboom-Gill (CPMG) ^{15}N-relaxation dispersion experiments (31) at 600 and 900 MHz. These experiments probe exchange dynamics between species with distinct chemical shifts on a time scale ranging from ~50 μs to 10 ms. Significant relaxation dispersion was observed for the backbone amides of a number of residues in the vicinity of the PEP binding site: Ile426 and Gly427 at the N-terminal end of strand β5; Arg465 and Asn467 located in the turn/loop (residues 453-477) connecting strand β6 to helix α6; and Gly337, Lys340, Glu341, Leu355, Trp357, Arg358 and Ala359 located in the turn/loop (residues 333-366) connecting strand β3 to helix α3 (Fig. 2B). Three of the residues, Leu355, Trp357 and Asn467, are also located at the dimer interface (Fig. 2C). The ^{15}N-relaxation dispersion curves for all the above residues at both fields (600 and 900 MHz) were fit simultaneously to a two-state model (Eq. 1 in *Experimental Procedures*) describing the interconversion of two conformational states, optimizing the values of the exchange rate (k_{ex}), the fractional population of the minor state (p_B), and the residue-specific ^{15}N chemical shift differences between the two conformational states ($\Delta\omega_N$). An example of the fits is provided in Fig. 2E and a summary of the results is provided in Table 1. The population of the minor species is ~3%, and the overall exchange rate (sum of forward and backward rate constants) is ~1500 s^{-1}. These parameters yield values of the rate constants for the conversion from the major to the minor species and from the minor to the major species of ~50 and ~1500 s^{-1}, respectively.

Consistent with the relaxation dispersion results, an overlay of the crystal structures of the EIC domain (15,16,26-28) obtained to date (Fig. 2D) shows that the backbone of the Gly337-Tyr344 segment of the β3α3 turn can adopt one of two conformations: an open state observed in the crystal structures of both free EI (from *S. aureus* and *S. carnosus*) and the isolated *T. Teng-congensis* EIC domain (free and bound to PEP or pyruvate) (cyan tubes in Fig. 2D); and a closed state found in the crystal structure of the trapped phosphorylated intermediate of E. coli EI (red tube in Fig. 2D). The closed state is stabilized by hydrogen bonds from the backbone amide groups of Gly337 and Ala359 to the backbone carbonyls Lys340 and Ile336, respectively. Both these hydrogen bonds are absent in the open state found in the crystal structure of *S. aureus* EI (16), and the Gly337→Lys340 hydrogen bond is missing in all crystal structures of the open state (16,26-28). Of note is that among the residues of the β3α3 turn displaying relaxation dispersion, Gly337 and Ala359 show the largest $\Delta\omega_N$ values (Table 1), suggesting that the exchange process detected by the relaxation dispersion experiments corresponds to the open/closed transition The conformational dynamics detected in the β3α3 turn extend all the way to the dimer interface, also affecting Arg465 and Asn467 that directly face the β3α3 turn in the other subunit (Figs. 2B and C).

Effect of PEP on the spectrum of EIC — Addition of 10 mM PEP to EIC results in substantial changes in the ^{1}H-^{15}N TROSY spectrum (Fig. 3A). However, as we discuss in depth in a subsequent section, we noticed that formation of the EIC-PEP complex also results in degradation of PEP into pyruvate and inorganic

Downloaded from www.jbc.org at National Institutes of Health Library, on June 21, 2012

phosphate, making the lifetime of the EIC-PEP complex too short (<4 hours at 37°C with 400 μM EIC and 10 mM PEP) to allow acquisition of the 3D triple resonance experiments necessary for sequential backbone resonance assignment. Thus, only those ^{1}H-^{15}N cross-peaks that could be unambiguously tracked in a PEP titration experiment were assigned in the EIC-PEP complex and used for further analysis.

The assigned backbone amides for the EIC-PEP complex and the corresponding $^{1}H/^{15}N$ chemical shift perturbations ($\Delta_{H/N}$) arising from PEP binding are depicted on the EIC structure in Fig. 3B. Although the ^{1}H-^{15}N cross-peaks of residues directly facing PEP are completely broadened out after addition of ligand, large $\Delta_{H/N}$ values are still observed for the flanking residues (Ile275, Gly276, Ile426, and Gly427) suggesting that structural rearrangements are occurring at the active site (Figs. 3B and D). Moreover, the ^{1}H-^{15}N cross-peaks of residues in the β3α3 turn experience extensive line broadening upon addition of PEP (Fig. 3C), indicating that the binding of the substrate affects the conformational dynamics detected in this area.

The perturbations on the ^{15}N chemical shifts ($\Delta\delta_N$) of EIC observed upon PEP binding are in excellent agreement with the $|\Delta\omega_N|$ values obtained from the relaxation dispersion measurements on free EIC (Table 1), strongly suggesting that binding of PEP shifts the conformational equilibrium detected in free EIC from the open to the closed state. This is consistent with the model of the *E. coli* EIC-PEP complex (Fig. 2B), derived from the structures of *E. coli* phosphorylated EI (15) and the *T. Tengcongensis* EIC-PEP complex (28), which shows that salt bridges between the phosphate group of PEP and the side chains of Lys340 and Arg358 lock the β3α3 turn in the closed conformation, providing further stabilization to the Gly337→Lys340 and Ala359→Ile336 backbone hydrogen bonds. These key interactions, together with an additional salt bridge between the phosphoryl group of PEP and the guanadino group of Arg465 (Fig. 2B), also serve to stabilize the backbone conformation of Leu355, Trp357, and Asn467 in the closed state observed in the X-ray structure of phosphorylated EI. Since Leu355, Trp357, and Asn467 are involved in several intersubunit contacts (Fig. 2C), the above observations explain the lower dimerization K_D measured for EI in the presence of PEP (22), as well as the large $\Delta_{H/N}$ perturbations induced by PEP for Glu351, Asn352, Gly356, and Trp357 in the β3α3 turn, and for Arg465, Asp468, Ile470 and Asn475 at the dimer interface (Figs. 3B and C). In addition, the β3α3 turn is rich in aromatic residues (Tyr344, Phe347, Phe354, and Trp357) so that conformational rearrangements in this region are fully consistent with the changes observed in the CD and fluorescence spectra of EIC upon PEP binding (14).

Effect of PEP on the quaternary structure of EIC — To assess whether the local conformational changes in the β3α3 turn observed in EIC upon PEP binding affect the subunit orientation in the EIC dimer, backbone amide ($^{1}D_{NH}$) residual dipolar couplings (RDCs) for well resolved ^{1}H-^{15}N cross-peaks were measured on samples of weakly aligned EIC and the EIC-PEP complex in a dilute liquid crystalline medium of phage *pf1* (39). To avoid structural noise from flexible regions, only the backbone amides from secondary structure elements were included in the analysis. This necessary precaution, together with the fact that a low protein concentration was used in the EIC-PEP sample to limit the rate of PEP hydrolysis, reduced the number the experimental RDCs available for the EIC-PEP complex to 37 (Table 2). However, since $^{1}D_{NH}$ RDCs provide orientational information on NH bond vectors relative to an external alignment tensor (38,50), the subunit structure of EIC is known and one of the principal components of the alignment tensor must lie along the C_2 symmetry axis of the dimer (17), this small number of RDCs is sufficient to fully describe the relative orientation of the two symmetry-related subunits (51).

Singular value decomposition (SVD) fitting of the experimental $^{1}D_{NH}$ RDCs to the coordinates of a single subunit from the phosphorylated EI X-ray structure (15) yields RDCs R-factors (52) of less than 22% for both EIC and the EIC-PEP complex (Fig. 4 and Table 2), confirming that the tertiary subunit fold of the secondary structure elements is unchanged relative to the crystal structure. The decrease in both the axial component of the alignment tensor, D_a, and the rhombicity upon addition of PEP (Table 2) reflects changes in the surface charge distribution arising from the presence of PEP.

When the RDCs measured for EIC and the EIC-PEP complex are fitted to coordinates of the dimer, the RDC R-factors increase by less than 1% (reflecting the doubling of the number of RDCs), and only minor variations within

Downloaded from www.jbc.org at National Institutes of Health Library, on June 21, 2012

experimental error are observed in the Euler angles (Table 2), relative to the fits obtain with an individual subunit. These data demonstrate unambiguously, that although PEP binding results in local conformational changes within the active site and β3α3 turn, the relative subunit orientation within the dimer is unaffected by the substrate, and is the same as that observed in the various crystal structures.

Enzymatic activity of E. coli EIC - During the course of our NMR studies on the EIC-PEP complex, we noticed that the ^{1}H-^{15}N TROSY correlation spectrum for the EIC-PEP complex changes over time and slowly reverts to that of the free protein, indicating that EIC degrades PEP and that the degradation products are no longer able to interact with the protein. This is confirmed by ^{31}P NMR which shows that a 100 μM EIC sample is able to fully hydrolyze 10 mM PEP into phosphate and pyruvate in less than 16 h (Fig. 5A). Similar results are obtained with full-length EI (Fig. 5A).

An enzymatic assay that detects the amount of inorganic phosphate released as a consequence of PEP degradation (see *Experimental Procedures*), reveals that the hydrolysis of PEP by both EI and EIC follows Michaelis-Menten kinetics with K_m values of 327 and 374 μM, respectively (Fig. 5B and Table 3). These values agree well with the previously reported K_m (~ 400 μM) for the EI-PEP interaction (20), and indicate that the isolated EIC domain binds PEP with essentially the same affinity as the full-length protein.

Differences, however, are observed for the EI and EIC kinetics, with full length EI hydrolyzing PEP with ~ 1.5 times higher efficiency (reported as k_{cat}/K_m in Table 3) than the isolated EIC domain. A schematic diagram for the PEP degradation pathways catalyzed by EI and EIC is shown in Fig. 5C. The autophosphorylation reaction (equilibrium *d* in Fig. 5C), that initiates the PTS, and occurs in only the full-length protein, is ~6 order of magnitude faster than the direct hydrolysis of PEP into pyruvate and inorganic phosphate catalyzed by EIC (equilibria *a* and *c* in Fig. 5C). Phosphorylated EI, that is rapidly formed after addition of PEP to the full-length protein, can generate inorganic phosphate through two independent pathways that occur with similar velocities (equilibria *e* and *f* in Fig. 5C), explaining the higher efficiency of PEP degradation exhibited by the full-length protein relative to EIC.

It is also worth noting that no hydrolysis of PEP by EIC purified from species 1 (see section on *expression and isolation of recombinant E. coli EIC* and Figs. 1A and B) could be detected by the enzymatic assay (Table 3), further confirming that species 1 is an inactive EIC isoform.

Concluding remarks — Binding of PEP to the EIC domain of EI initiates the PTS (9) by inducing a series of intra and inter-domain conformational rearrangements (15,17) that results in phosphorylation of EIN and subsequent transfer of the phosphoryl group to HPr. Although conformational changes in EIC are thought to play an important role in regulation of the overall PTS (14,22), the conformations adopted by EIC during catalysis are still poorly understood.

We have presented a protocol for the successful expression and purification of recombinant EIC from *E. coli*. NMR structural characterization shows that in solution EIC adopts the same tertiary fold and dimeric structure as that observed in the various crystal structures of EI (15,16,26) and EIC (27,28). NMR ^{15}N relaxation dispersion data also reveal the existence of conformational exchange on the sub-millisecond time scale in the region of the PEP binding and at the β3α3 turn. The relaxation dispersion data together with the available crystal structures of EI and EIC suggest that the β3α3 turn in free EIC exists in a dynamic conformational equilibrium between open (major) and closed (minor) states that is shifted toward the closed state upon PEP binding. Conformational selection of the closed state by PEP does not perturb the quaternary structure and relative subunit orientation in the dimer but stabilizes the dimer interface, thereby explaining the lower dimerization K_D for EIC in the presence of PEP (14).

We have also shown that the EIC domain, both isolated and in the context of the full-length protein, is able to hydrolyze PEP into pyruvate and inorganic phosphate, further supporting the hypothesis that EIC is not merely a scaffold for PEP binding and a dimerization domain, but actually plays an active role in the catalytic function of EI (12). Although this enzymatic activity was not reported in previous investigations on the isolated EIC domain from *E. coli* (14), our finding is not too surprising since the isolated EIC domain from *T. Tengcongensis* was observed to catalyze a similar reaction at 65°C (28). Our data also indicate that EI is capable of hydrolyzing PEP even when phosphorylated at His189. However, the PEP

Downloaded from www.jbc.org at National Institutes of Health Library, on June 21, 2012

degradation rate is ~6 order of magnitude slower than the autophosphorylation reaction of EI (21), suggesting that this additional processing of PEP is negligible in the context of the full PTS.

We expect that the stable and active EIC domain expressed and purified here will serve as an excellent model system for biochemical and structural investigations on the complex interplay between substrate binding and conformational dynamics that regulates EI and, more generally, the activity of many enzymes (53).

Acknowledgments

We thank Drs. Nicolas Fawzi, Nicolas Anthis, Yuki Takayama, Sara Pistolesi, Alexander Maltsev, and Nils Lakomek for helpful discussions. This work was supported by funds from the Intramural Program of the NIH, NIDDK, and the Intramural AIDS Targeted Antiviral Program of the Office of the Director of the NIH (to G.M.C.).

Downloaded from www.jbc.org at National Institutes of Health Library, on June 21, 2012

[1]**Abbreviations:** EI, enzyme I (residues 1-575); EIN, N-terminal domain of EI (residues 1-249); EIC, C-terminal domain of EI (residues 261-575); PTS, phosphoenolpyruvate:sugar phosphotransferase system; PEP, phosphoenolpyruvate; HPr, histidine phosphocarrier protein; LB medium, Luria Bertani medium; DTT, dithiotreitol; EDTA, ethylenediaminetetraacetic acid; PMSF, phenylmethylsulfonyl fluoride; ;TROSY, transverse relaxation optimized spectroscopy; RDCs, residual dipolar couplings; SVD, singular value decomposition; CPMG experiment, Carr-Purcel-Meinboom-Gill experiment; ARTSY, *a*mide *R*DCs by *TR*OSY *s*pectroscopy; $^{1}D_{NH}$, one-bond backbone amide RDCs

References

1. Meadow, N. D., Fox, D. K., and Roseman, S. (1990) The bacterial phosphoenolpyruvate: glycose phosphotransferase system. *Annu. Rev. Biochem.* **59**, 497-542
2. Deutscher, J., Francke, C., and Postma, P. W. (2006) How phosphotransferase system-related protein phosphorylation regulates carbohydrate metabolism in bacteria. *Microbiol. Mol. Biol. Rev.* **70**, 939-1031
3. Weigel, N., Waygood, E. B., Kukuruzinska, M. A., Nakazawa, A., and Roseman, S. (1982) Sugar transport by the bacterial phosphotransferase system. Isolation and characterization of enzyme I from Salmonella typhimurium. *J. Biol. Chem.* **257**, 14461-14469
4. Weigel, N., Kukuruzinska, M. A., Nakazawa, A., Waygood, E. B., and Roseman, S. (1982) Sugar transport by the bacterial phosphotransferase system. Phosphoryl transfer reactions catalyzed by enzyme I of Salmonella typhimurium. *J. Biol. Chem.* **257**, 14477-14491
5. Doucette, C. D., Schwab, D. J., Wingreen, N. S., and Rabinowitz, J. D. (2011) alpha-Ketoglutarate coordinates carbon and nitrogen utilization via enzyme I inhibition. *Nature Chem. Biol.* **7**, 894-901
6. Mukhija, S., and Erni, B. (1997) Phage display selection of peptides against enzyme I of the phosphoenolpyruvate-sugar phosphotransferase system (PTS). *Mol. Microbiol.* **25**, 1159-1166
7. Chauvin, F., Brand, L., and Roseman, S. (1994) Sugar transport by the bacterial phosphotransferase system. Characterization of the Escherichia coli enzyme I monomer/dimer transition kinetics by fluorescence anisotropy. *J. Biol. Chem.* **269**, 20270-20274
8. Chauvin, F., Fomenkov, A., Johnson, C. R., and Roseman, S. (1996) The N-terminal domain of Escherichia coli enzyme I of the phosphoenolpyruvate/glycose phosphotransferase system: molecular cloning and characterization. *Proc. Natl. Acad. Sci. U. S. A.* **93**, 7028-7031
9. Chauvin, F., Brand, L., and Roseman, S. (1996) Enzyme I: the first protein and potential regulator of the bacterial phosphoenolpyruvate: glycose phosphotransferase system. *Res. Microbiol.* **147**, 471-479
10. Liao, D. I., Silverton, E., Seok, Y. J., Lee, B. R., Peterkofsky, A., and Davies, D. R. (1996) The first step in sugar transport: crystal structure of the amino terminal domain of enzyme I of the E. coli PEP: sugar phosphotransferase system and a model of the phosphotransfer complex with HPr. *Structure* **4**, 861-872

11. Garrett, D. S., Seok, Y. J., Liao, D. I., Peterkofsky, A., Gronenborn, A. M., and Clore, G. M. (1997) Solution structure of the 30 kDa N-terminal domain of enzyme I of the Escherichia coli phosphoenolpyruvate:sugar phosphotransferase system by multidimensional NMR. *Biochemistry* **36**, 2517-2530
12. Seok, Y. J., Lee, B. R., Zhu, P. P., and Peterkofsky, A. (1996) Importance of the carboxyl-terminal domain of enzyme I of the Escherichia coli phosphoenolpyruvate: sugar phosphotransferase system for phosphoryl donor specificity. *Proc. Natl. Acad. Sci. U. S. A.* **93**, 347-351
13. Seok, Y. J., Zhu, P. P., Koo, B. M., and Peterkofsky, A. (1998) Autophosphorylation of enzyme I of the Escherichia coli phosphoenolpyruvate:sugar phosphotransferase system requires dimerization. *Biochem. Biophys. Res. Commun.* **250**, 381-384
14. Patel, H. V., Vyas, K. A., Mattoo, R. L., Southworth, M., Perler, F. B., Comb, D., and Roseman, S. (2006) Properties of the C-terminal domain of enzyme I of the Escherichia coli phosphotransferase system. *J. Biol. Chem.* **281**, 17579-17587
15. Teplyakov, A., Lim, K., Zhu, P. P., Kapadia, G., Chen, C. C., Schwartz, J., Howard, A., Reddy, P. T., Peterkofsky, A., and Herzberg, O. (2006) Structure of phosphorylated enzyme I, the phosphoenolpyruvate:sugar phosphotransferase system sugar translocation signal protein. *Proc. Natl. Acad. Sci. U. S. A.* **103**, 16218-16223
16. Oberholzer, A. E., Schneider, P., Siebold, C., Baumann, U., and Erni, B. (2009) Crystal structure of enzyme I of the phosphoenolpyruvate sugar phosphotransferase system in the dephosphorylated state. *J. Biol. Chem.* **284**, 33169-33176
17. Schwieters, C. D., Suh, J. Y., Grishaev, A., Ghirlando, R., Takayama, Y., and Clore, G. M. (2010) Solution structure of the 128 kDa enzyme I dimer from Escherichia coli and its 146 kDa complex with HPr using residual dipolar couplings and small- and wide-angle X-ray scattering. *J. Am. Chem. Soc.* **132**, 13026-13045
18. Takayama, Y., Schwieters, C. D., Grishaev, A., Ghirlando, R., and Clore, G. M. (2011) Combined use of residual dipolar couplings and solution X-ray scattering to rapidly probe rigid-body conformational transitions in a non-phosphorylatable active-site mutant of the 128 kDa enzyme I dimer. *J. Am. Chem. Soc.* **133**, 424-427
19. Waygood, E. B., Meadow, N. D., and Roseman, S. (1979) Modified assay procedures for the phosphotransferase system in enteric bacteria. *Anal. Biochem.* **95**, 293-304
20. Saier, M. H., Jr., Schmidt, M. R., and Lin, P. (1980) Phosphoryl exchange reaction catalyzed by enzyme I of the bacterial phosphoenolpyruvate: sugar phosphotransferase system. Kinetic characterization. *J. Biol. Chem.* **255**, 8579-8584
21. Meadow, N. D., Mattoo, R. L., Savtchenko, R. S., and Roseman, S. (2005) Transient state kinetics of Enzyme I of the phosphoenolpyruvate:glycose phosphotransferase system of Escherichia coli: equilibrium and second-order rate constants for the phosphotransfer reactions with phosphoenolpyruvate and HPr. *Biochemistry* **44**, 12790-12796
22. Patel, H. V., Vyas, K. A., Savtchenko, R., and Roseman, S. (2006) The monomer/dimer transition of enzyme I of the Escherichia coli phosphotransferase system. *J. Biol. Chem.* **281**, 17570-17578
23. Rohwer, J. M., Meadow, N. D., Roseman, S., Westerhoff, H. V., and Postma, P. W. (2000) Understanding glucose transport by the bacterial phosphoenolpyruvate:glycose phosphotransferase system on the basis of kinetic measurements in vitro. *J. Biol. Chem.* **275**, 34909-34921
24. Suh, J. Y., Cai, M., and Clore, G. M. (2008) Impact of phosphorylation on structure and thermodynamics of the interaction between the N-terminal domain of enzyme I and the histidine phosphocarrier protein of the bacterial phosphotransferase system. *J. Biol. Chem.* **283**, 18980-18989
25. Garrett, D. S., Seok, Y. J., Peterkofsky, A., Gronenborn, A. M., and Clore, G. M. (1999) Solution structure of the 40,000 Mr phosphoryl transfer complex between the N-terminal domain of enzyme I and HPr. *Nature Struct. Biol.* **6**, 166-173
26. Marquez, J., Reinelt, S., Koch, B., Engelmann, R., Hengstenberg, W., and Scheffzek, K. (2006) Structure of the full-length enzyme I of the phosphoenolpyruvate-dependent sugar phosphotransferase system. *J. Biol. Chem.* **281**, 32508-32515
27. Oberholzer, A. E., Bumann, M., Schneider, P., Bachler, C., Siebold, C., Baumann, U., and Erni, B. (2005) Crystal structure of the phosphoenolpyruvate-binding enzyme I-domain from the Thermoanaerobacter tengcongensis PEP: sugar phosphotransferase system (PTS). *J. Mol. Biol.* **346**, 521-532

Downloaded from www.jbc.org at National Institutes of Health Library, on June 21, 2012

28. Navdaeva, V., Zurbriggen, A., Waltersperger, S., Schneider, P., Oberholzer, A. E., Bahler, P., Bachler, C., Grieder, A., Baumann, U., and Erni, B. (2011) Phosphoenolpyruvate: sugar phosphotransferase system from the hyperthermophilic Thermoanaerobacter tengcongensis. *Biochemistry* **50**, 1184-1193
29. LiCalsi, C., Crocenzi, T. S., Freire, E., and Roseman, S. (1991) Sugar transport by the bacterial phosphotransferase system. Structural and thermodynamic domains of enzyme I of Salmonella typhimurium. *J. Biol. Chem.* **266**, 19519-19527
30. Palmer, A. G., 3rd. (2004) NMR characterization of the dynamics of biomacromolecules. *Chem. Rev.* **104**, 3623-3640
31. Mittermaier, A., and Kay, L. E. (2006) New tools provide new insights in NMR studies of protein dynamics. *Science* **312**, 224-228
32. Delaglio, F., Grzesiek, S., Vuister, G. W., Zhu, G., Pfeifer, J., and Bax, A. (1995) NMRPipe: a multidimensional spectral processing system based on UNIX pipes. *J. Biomol. NMR* **6**, 277-293
33. Pervushin, K., Riek, R., Wider, G., and Wuthrich, K. (1997) Attenuated T_2 relaxation by mutual cancellation of dipole-dipole coupling and chemical shift anisotropy indicates an avenue to NMR structures of very large biological macromolecules in solution. *Proc. Natl. Acad. Sci. U. S. A.* **94**, 12366-12371
34. Tugarinov, V., Muhandiram, R., Ayed, A., and Kay, L. E. (2002) Four-dimensional NMR spectroscopy of a 723-residue protein: chemical shift assignments and secondary structure of malate synthase g. *Journal of the American Chemical Society* **124**, 10025-10035
35. Clore, G. M., and Gronenborn, A. M. (1998) Determining the structures of large proteins and protein complexes by NMR. *Trends Biotechnol.* **16**, 22-34
36. Ulrich, E. L., Akutsu, H., Doreleijers, J. F., Harano, Y., Ioannidis, Y. E., Lin, J., Livny, M., Mading, S., Maziuk, D., Miller, Z., Nakatani, E., Schulte, C. F., Tolmie, D. E., Kent Wenger, R., Yao, H., and Markley, J. (2008) BioMagResBank. *Nucleic Acids Res.* **36**, D402-D408
37. Mulder, F. A., Schipper, D., Bott, R., and Boelens, R. (1999) Altered flexibility in the substrate-binding site of related native and engineered high-alkaline Bacillus subtilisins. *J. Mol. Biol.* **292**, 111-123
38. Bax, A., Kontaxis, G., and Tjandra, N. (2001) Dipolar couplings in macromolecular structure determination. *Methods Enzymol.* **339**, 127-174
39. Clore, G. M., Starich, M. R., and Gronenborn, A. M. (1998) Measurement of residual dipolar couplings of macromolecules aligned in the nematic phase of a colloidal suspension of rod-shaped viruses. *J. Am. Chem. Soc.* **120**, 10571–10572
40. Hansen, M. R., Mueller, L., and Pardi, A. (1998) Tunable alignment of macromolecules by filamentous phage yields dipolar coupling interactions. *Nature Struct. Biol.* **5**, 1065-1074
41. Fitzkee, N. C., and Bax, A. (2011) Facile measurement of ^{1}H-^{15}N residual dipolar couplings in larger perdeuterated proteins. *J. Biomol. NMR* **48**, 65-70
42. Schwieters, C. D., Kuszewski, J., and Clore, G. M. (2006) Using Xplor–NIH for NMR molecular structure determination. *Progr Nucl Magn Reson Spect* **48**, 47–62
43. Loria, J. P., Rance, M., and Palmer, A. G., 3rd. (1999) A TROSY CPMG sequence for characterizing chemical exchange in large proteins. *J. Biomol. NMR* **15**, 151-155
44. Yip, G. N., and Zuiderweg, E. R. (2004) A phase cycle scheme that significantly suppresses offset-dependent artifacts in the R2-CPMG 15N relaxation experiment. *J Magn Reson* **171**, 25-36
45. Mulder, F. A., Skrynnikov, N. R., Hon, B., Dahlquist, F. W., and Kay, L. E. (2001) Measurement of slow (micros-ms) time scale dynamics in protein side chains by (15)N relaxation dispersion NMR spectroscopy: application to Asn and Gln residues in a cavity mutant of T4 lysozyme. *J. Am. Chem. Soc.* **123**, 967-975
46. Davis, D. G., Perlman, M. E., and London, R. E. (1994) Direct measurements of the dissociation-rate constant for inhibitor-enzyme complexes via the $T_{1\rho}$ and T_2 (CPMG) methods. *J. Magn. Reson. Ser. B* **104**, 266-275
47. Millet, O., Loria, J. P., Kroenke, C. D., Pons, M., and Palmer, A. G., 3rd. (2000) The static magnetic field dependence of chemical exchange linebroadening defines the NMR chemical shift time scale. *J. Am. Chem. Soc.* **122**, 2867-2877
48. Venditti, V., Fawzi, N. L., and Clore, G. M. (2011) An efficient protocol for incorporation of an unnatural amino acid in perdeuterated recombinant proteins using glucose-based media. *J. Biomol. NMR* **52**, 191-195
49. Shen, Y., Delaglio, F., Cornilescu, G., and Bax, A. (2009) TALOS+: a hybrid method for predicting protein backbone torsion angles from NMR chemical shifts. *J. Biomol. NMR* **44**, 213-223
50. Prestegard, J. H., al-Hashimi, H. M., and Tolman, J. R. (2000) NMR structures of biomolecules using field oriented media and residual dipolar couplings. *Q. Rev. Biophys.* **33**, 371-424

Downloaded from www.jbc.org at National Institutes of Health Library, on June 21, 2012

51. Clore, G. M. (2000) Accurate and rapid docking of protein-protein complexes on the basis of intermolecular nuclear overhauser enhancement data and dipolar couplings by rigid body minimization. *Proc. Natl. Acad. Sci. U. S. A.* **97**, 9021-9025
52. Clore, G. M., and Garrett, D. S. (1999) R-factor, free R and complete cross-validation for dipolar coupling refinement of NMR structures. *J. Am. Chem. Soc.* **121**, 9008-9012
53. Ma, B., and Nussinov, R. (2010) Enzyme dynamics point to stepwise conformational selection in catalysis. *Curr. Opin. Chem. Biol.* **14**, 652-659

Figure Legends

Fig. 1. Isolation and purification of *E. coli* EIC. *A*, Size exclusion chromatography elution profile. *B* and *C*, Chromatograms of the final anion exchange step obtained for species 1 and 2, respectively. The salt gradient is shown in *red*. *D* and *E*, 600 MHz ^{1}H-^{15}N TROSY correlation spectra obtained for EIC from species 1 and 2, respectively. Buffer conditions are as described in *Experimental Procedures*. *F*, Selected regions of the ^{1}H-^{15}N TROSY spectrum showing the overlap of EI (blue) and EIC (red) cross-peaks. The cross-peaks for the isolated EIN domain are displayed in green for completeness. NMR spectra for the isolated EIN and EIC domains were acquired at 600 MHz. The full-length EI spectrum was acquired at 900 MHz.

Fig. 2. Structure and dynamics of the free EIC domain. *A*, Correlation between the backbone ϕ/ψ torsion angles derived from backbone ^{1}H/^{15}N/^{13}C chemical shifts using the program TALOS+ (49) and those in the crystal structure of the trapped phosphorylated intermediate of intact *E. coli* EI. The data for loop regions (where conformational differences between solution and crystal are to be expected) are depicted as *open circles*, while the data for secondary structure elements are reported as *filled-in circles*. The overall correlation coefficient is 0.90, and the correlation coefficient computed using only the data from secondary structure elements is 0.95. *B*, Structural model for the *E. coli* EIC-PEP complex. The model was obtained by rigid-body least-square fitting of the backbone atoms of the X-ray structure of the EIC-PEP complex from *T. Tengcongensis* (28) onto the EIC coordinates of the X-ray structure of phosphorylated EI from *E. coli* (15). The fitting was carried out using residues 261-333 and 367-570, and the Cα rms difference is 1.1 Å. Ribbons of the two identical subunits are depicted in *yellow* and *white*. The PEP molecule is displayed as *green* bonds, and the side chains of Lys340, Arg358 and Arg465 are shown as *red* bonds. The nitrogen atoms of amide groups exhibiting significant ^{15}N relaxation dispersion, characteristic of dynamics on the sub-millisecond to millisecond timescale, are shown as *blue* spheres. The inset provides a close-up of the $\beta3\alpha3$ turn. The turn is highlighted in *cyan*, the carbonyl groups of Ile336 and Lys340 are shown as spheres (*gray* for carbon, *red* for oxygen), and the amide groups of residues in this region displaying relaxation dispersion are shown as spheres, *blue* for nitrogen and white for the associated amide proton. *C*, Close up view of the EIC dimer interface. The two subunits are colored in *white* and *yellow*. The atoms of Leu355, Trp357 and Asn467 are represented as red spheres. *D*, Superposition of the X-ray structures of EIC (15,16,26-28) illustrating the conformational variability in the $\beta3\alpha3$ turn. The $\beta3\alpha3$ turn in the closed conformation seen in the X-ray structure of phosphorylated EI is highlighted in *red*; in all the other cases the $\beta3\alpha3$turn is in the open conformation and colored in *cyan*. PEP is displayed as green bonds. The amide groups (*blue* for N, white for H_N) of Gly337 and Ala359, as well as the carbonyl groups (*red* for O, *grey* for C') of Ile336 and Lys340 (*red*), are shown as spheres on the phosphorylated EI structure. *E*, Examples of typical relaxation dispersion data at 600 MHz (left panel) and 900 MHz (right panel). Data are shown for Glu341 (*red*) and Ala359 (*blue*) with the experimental data represented by *filled-in circles* and the best-fit curves for a two-site exchange model as *solid lines*. The optimized values of the kinetic, population and chemical shift parameters derived from the relaxation dispersion data are provided in Table 1.

Downloaded from www.jbc.org at National Institutes of Health Library, on June 21, 2012

Fig. 3 Structure and dynamics of the EIC-PEP complex. *A*, 600 MHz ^{1}H-^{15}N TROSY correlation spectrum of EIC in the absence (*red*) and presence (*blue*) of 10 mM PEP. *B*, Structural model for the EIC-PEP complex (see Fig. 2 caption) showing the extent of $^{1}H_N/^{15}N$ chemical shift perturbation ($\Delta_{H/N}$; see *Experimental Procedures* for definition) upon addition of 10 mM PEP to the protein sample. Assigned backbone amides are depicted as spheres and colored according to their $\Delta_{H/N}$ values (color bar ranging from *blue* to *red*). Amide groups assigned only for free EIC are displayed as *grey* spheres. The inset shows a close-up of the dimer interface. The amide groups exhibiting $\Delta_{H/N}$ values > 0.2 ppm are displayed as spheres. *C*, Selected regions of the ^{1}H-^{15}N TROSY spectrum of EIC showing the effect of increasing concentrations of PEP on cross-peaks originating from residues in the β3α3 turn. The color code is as follows: *red*, 0 mM PEP; *green*, 0.2 mM PEP; *yellow*, 0.4 mM PEP; *purple*, 1 mM PEP; *blue*, 10 mM PEP. It should be noted that since PEP is hydrolyzed by EIC (see main text) the listed PEP concentrations are approximate values. *D*, $\Delta_{H/N}$ profile.

Fig. 4. RDC analysis of free EIC and the EIC-PEP complex. *A*, Free EIC. *B*, EIC-PEP complex. The two panels show a comparison of the observed and calculated RDCs obtained by SVD to the coordinates of an individual subunit of EIC (*blue open circles*) and the EIC dimer (*red filled-in circles*). The coordinates of the X-ray structure of phosphorylated EI from *E. coli* were used (15).

Fig. 5 Enzymatic activity of EIC. *A*, ^{31}P NMR spectra showing hydrolysis of PEP catalyzed by EI and EIC. The *blue* spectra were acquired on 100 μM samples of EI (*left panel*) and EIC (*right panel*) immediately after addition of 10 mM PEP. The red spectra were acquired after 16 h of incubation at 37°C at which time all the PEP has been hydrolyzed to inorganic phosphate and pyruvate. *B*, Michaelis-Menten kinetics for EI (*blue*) and EIC (*red*) with the substrate PEP. *C*, Schematic diagram showing the possible PEP degradation pathways by EIC (*top*) and EI (*bottom*). For each equilibrium the velocity of the forward reaction is provided. Velocities for the equilibria *a*, *b*, *c*, and *f* were calculated based on the k_{cat}/K_m values reported in Table 3 for EI (*b*) and EIC (*a, c* and *f*). The velocity for the equilibrium *d* was calculated based on the second-order rate constant obtained for the EI autophosphorylation reaction at 25°C (21). The velocity for the equilibrium *e* was calculated based on the half-life ($t_{1/2}$) for the decay of phosphorylated EI to unphosphorylated EI reported by Suh et al. (24). For all the conversions, K_m was set to 350 μM and the EI concentration to 5 μM.

Downloaded from www.jbc.org at National Institutes of Health Library, on June 21, 2012

Table 1

Kinetic, population and chemical shift parameters for conformational exchange between open and closed states of EIC derived from relaxation dispersion experiments.

All the relaxation dispersion curves at two fields (600 and 900 MHz) are fit simultaneously to a two-site exchange model, optimizing the values of two global parameters, the overall exchange rate (k_{ex}) and the population of the minor state (p_B), and the residue specific $|\Delta\omega_N|$ values which represent the absolute ^{15}N chemical shift difference between the major and minor states.

	G337	K340	E341	L355	W357	R358	A359	I426	G427	R465	N467
Global parameters											
k_{ex} (s^{-1})					1520±350						
p_B (%)					3±1						
k_{AB} (s^{-1})[a]					46±26						
k_{BA} (s^{-1})[a]					1474±385						
Residue specific parameters											
$\|\Delta\omega_N\|$ (ppm)[b]	2.0	0.6	1.0	1.1	1.0	0.7	2.0	1.9	2.0	0.8	0.8
^{15}N chemical shift perturbation from PEP titration experiment											
$\Delta\delta_N$ (ppm)[c]	0.9[d]	-	1.3	-	-	-	-	2.3	2.2	1.3	-

[a] The open (major) and closed (minor) states are referred to as A and B. k_{AB} and k_{BA} are the rate constants for the transition from A to B, and from B to A, respectively, and are calculated from the values of the optimized parameters k_{ex} (= k_{AB} + k_{BA}) and p_B.

[b] The error in the values of $|\Delta\omega_N|$ is ±0.1 ppm with the exception of those for Leu355 and Arg465 which are ±0.2 ppm.

[c] ^{15}N chemical shift perturbations upon addition of 10 mM PEP are provided for comparison with the values of $|\Delta\omega_N|$ obtained from the relaxation dispersion experiments on free EIC.

[d] The significant difference between $|\Delta\omega_N|$ and $\Delta\delta_N$ observed for Gly337 can be ascribed to the different conformations adopted by the side chain of Arg358 in free EIC and the EIC-PEP complex. In the crystal structures of free EIC, the guanidino group of Arg358 is located 4-5 Å away from the backbone amide of Gly337. However, in the structural model for the EIC-PEP complex displayed in Fig. 2, the Arg358 side chain directly interacts with PEP and the positively charged guanidino group is located more than 6 Å away from the backbone amide of Gly337. Since the relaxation dispersion experiments were acquired in the absence of substrate, the effect of this conformational change on the ^{15}N chemical shifts of EIC are observable in the $\Delta\delta_N$ values only.

Downloaded from www.jbc.org at National Institutes of Health Library, on June 21, 2012

Table 2

SVD analysis of $^1D_{NH}$ RDCs for the monomeric and dimeric forms of EIC and EIC-PEP.[a]

	monomer / dimer[b]						
	Number of RDCs	Euler angles (°)[c]			D_a (Hz)[c]	η[c]	R-factor (%)[d]
		ϕ	θ	ψ			
EIC	86/172	99/93	21/20	167/172	18.8/18.8	0.41/0.42	18.4/18.6
EIC-PEP	37/74	107/95	17/17	178/170	13.1/13.2	0.11/0.09	21.6/22.6

[a] The coordinates used for SVD analysis are those of EIC in the crystal structure of phosphorylated EI (15). The RDCs for the EIC-PEP complex were measured on samples containing 100 µM EIC and 50 mM PEP. The stability of the NMR samples used for measuring the RDCs was confirmed by acquiring ^{1}H-^{15}N TROSY spectra immediately before and after the acquisition of the ARTSY experiment.

[b] The first and second numbers listed give the results of the SVD fits to a single subunit and to the dimer.

[c] The alignment tensor is described by 5 parameters: three Euler angles (ϕ, θ and ψ), the magnitude of the alignment tensor D_a and the rhombicity η. For a symmetric dimer, one of the axes of the principal components of the alignment tensor coincides with the C_2 symmetry axis of the dimer. The fact that the values of the alignment tensor and RDC R-factor are the same for the SVD fits to a monomer and a dimer indicates that the orientation of the two subunits in the dimer in solution is the same as that in the crystal structure.

[d] The RDC R-factor is given by $[<(D_{obs} - D_{calc})^2>/(2<D_{obs}^2>]^{1/2}$, where D_{obs} and D_{calc} are the observed and calculated RDCs, respectively (52).

Table 3

Michaelis-Menten parameters for the hydrolysis of PEP into inorganic phosphate and pyruvate by EI and EIC.

	K_m (µM)	V_{max} (µmol s^{-1})	k_{cat} (s^{-1})	k_{cat} / K_m (M^{-1} s^{-1})
EI	328±25	383(±6)x10^{-8}	1.9(±1.5)x10^{-3}	5.9±1.7
EIC - species 2[a]	374±30	267(±5)x10^{-8}	1.3(±1.1)x10^{-3}	3.6±1.5
EIC - species 1[b]	-	<3x10^{-8}	-	-

[a] EIC purified from species 2 exhibits a well dispersed ^{1}H-^{15}N TROSY correlation spectrum typical of a folded protein (Fig. 1E).

[b] EIC purified from species 1 exhibits a ^{1}H-^{15}N TROSY correlation spectrum typical of an unfolded, partially folded or incorrectly folded protein with minimal chemical shift dispersion (Fig. 1D).

Downloaded from www.jbc.org at National Institutes of Health Library, on June 21, 2012

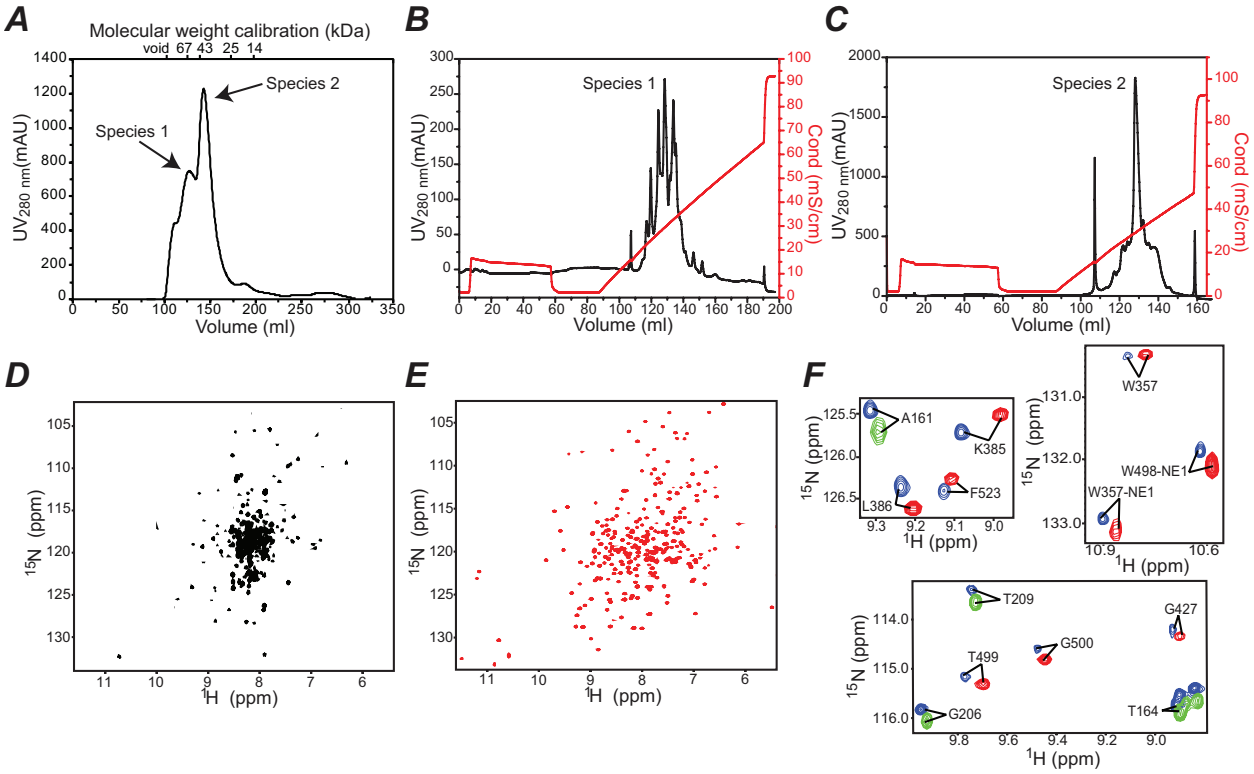

Fig. 1

Downloaded from www.jbc.org at National Institutes of Health Library, on June 21, 2012

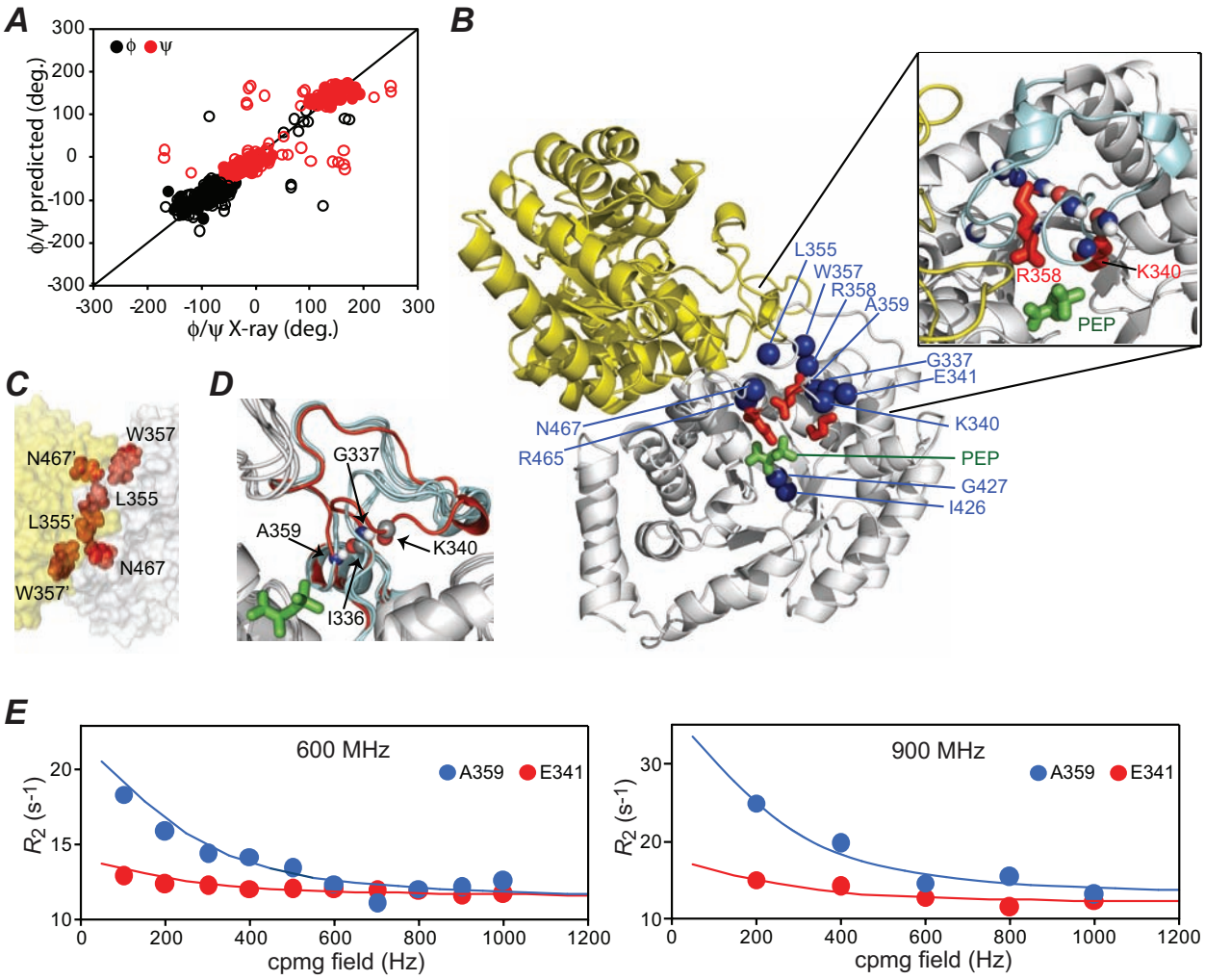

Fig. 2

Downloaded from www.jbc.org at National Institutes of Health Library, on June 21, 2012

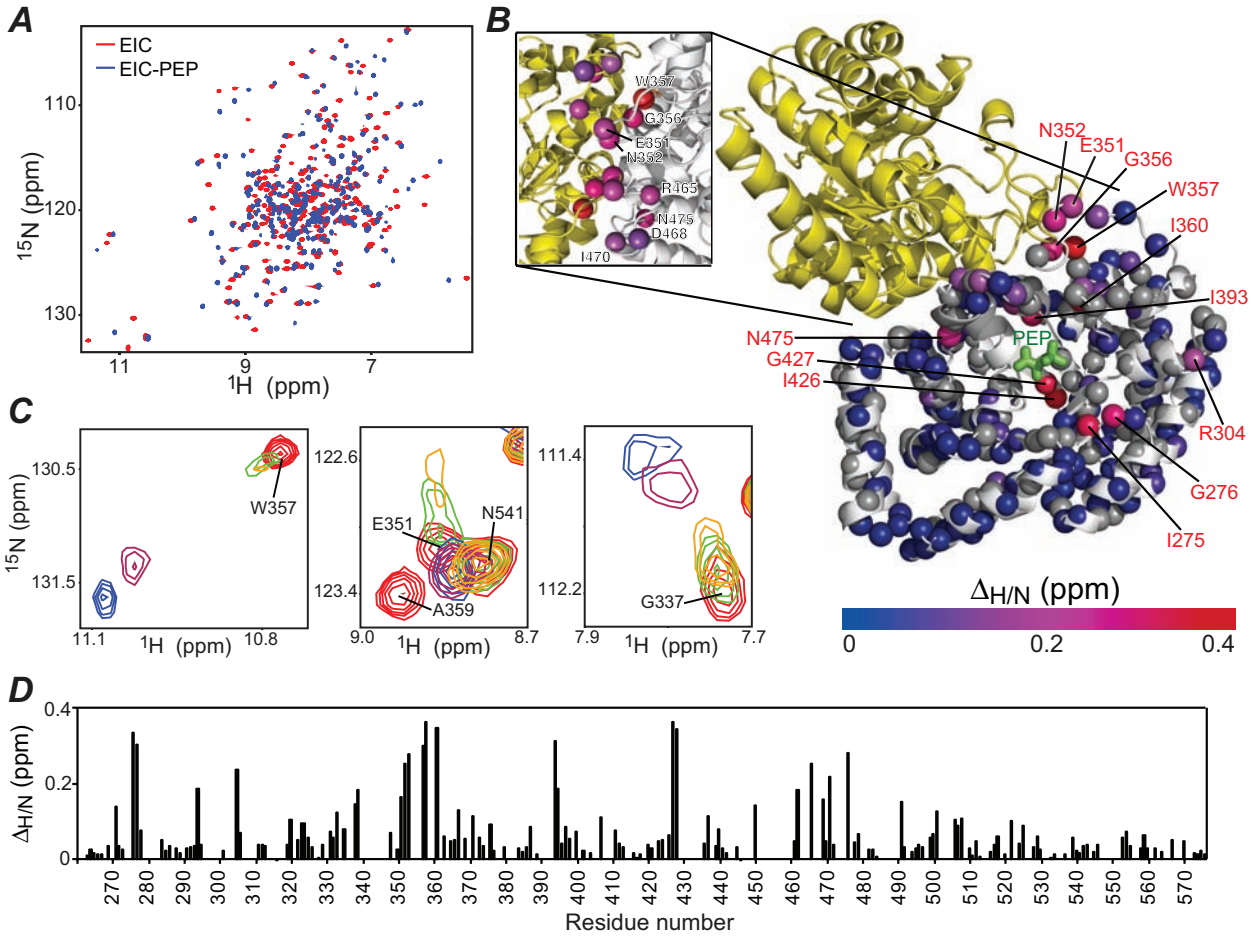

Fig. 3

Downloaded from www.jbc.org at National Institutes of Health Library, on June 21, 2012

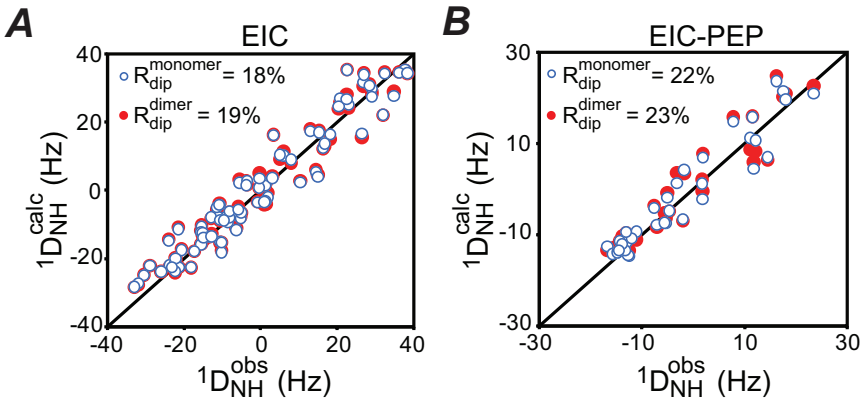

Fig. 4

Downloaded from www.jbc.org at National Institutes of Health Library, on June 21, 2012

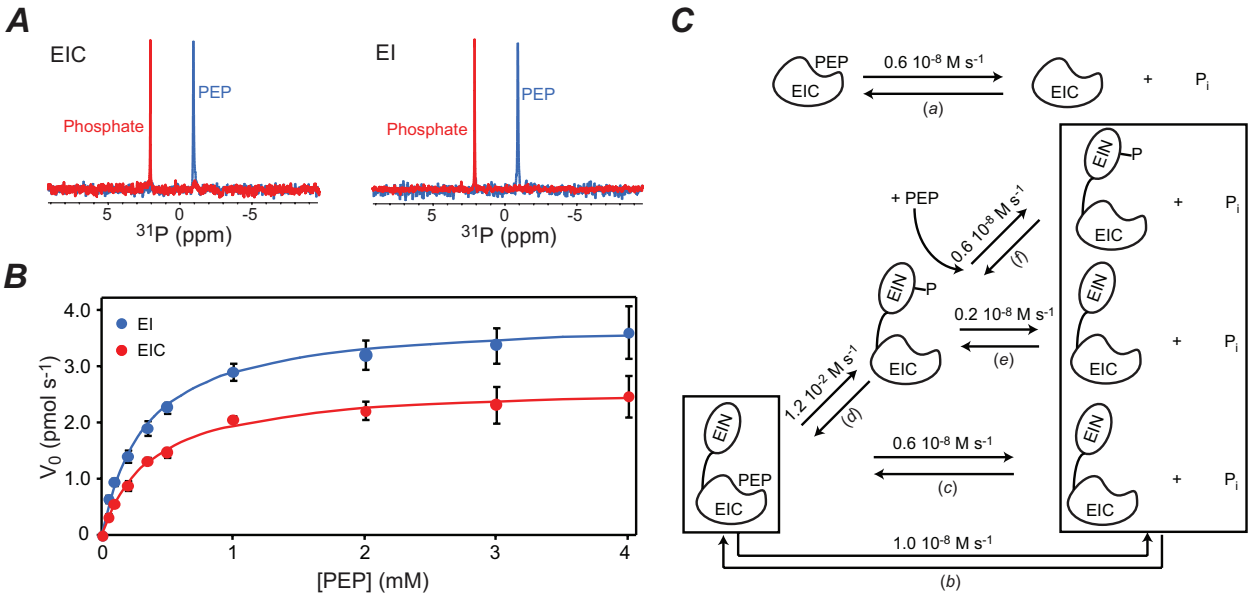

Fig. 5

Downloaded from www.jbc.org at National Institutes of Health Library, on June 21, 2012